

# Understanding Radar Refractivity: Sources of Uncertainty

David Bodine<sup>1,2</sup>, Dan Michaud<sup>1,2</sup>, Robert D. Palmer<sup>1,2</sup>, Pamela L. Heinselman<sup>3</sup>,  
Jerry Brotzge<sup>4</sup>, Nick Gasperoni<sup>1,4</sup>, Boon Leng Cheong<sup>2</sup>, Ming Xue<sup>4</sup>, and Jidong  
Gao<sup>4</sup>

<sup>1</sup>School of Meteorology, University of Oklahoma, Norman, OK, USA

<sup>2</sup>Atmospheric Radar Research Center, University of Oklahoma, Norman, OK,  
USA

<sup>3</sup>NOAA/OAR National Severe Storms Laboratory, Norman, OK, USA

<sup>4</sup>Center for Analysis and Prediction of Storms, Norman, OK, USA

March 24, 2011

*Corresponding author*

Dr. Robert Palmer

School of Meteorology

University of Oklahoma

120 David L. Boren Blvd., Suite 5900, Norman, OK 73072

E-mail: rpalmer@ou.edu

## Abstract

This study presents a two-year long validation of WSR-88D radar refractivity retrievals, and discusses some challenges to implementing radar refractivity operationally. Temporal and spatial analysis of radar refractivity exhibit high correlation with Oklahoma Mesonet data; however, periods of large refractivity differences are observed. Several sources of refractivity differences are examined to determine the cause of large refractivity differences. One source for non-klystron radars includes magnetron frequency drift, which can introduce errors up to 10 N-units if the frequency drift is not corrected. Different reference maps made at different times can “shift” refractivity values. A semi-automated method for producing reference maps is presented, including tradeoffs for making reference maps under different conditions. Refractivity from six Mesonet stations within the clutter domain of the Oklahoma City WSR-88D (KTLX) are compared to radar refractivity retrievals, including refractivity measurements at both 2 and 9 m at the Norman Mesonet site. The analysis revealed that the six Mesonet stations exhibited a prominent diurnal trend in refractivity difference, although some differences were noted among Mesonet stations. The diurnal range of the refractivity difference sometimes exceeded 20 or 30 N-units in the warm season, which translated to a potential dew point temperature bias of several degrees Celsius. A seasonal analysis revealed that large refractivity differences primarily occurred during the warm season when refractivity is most sensitive to moisture. Ultimately, the main factor in determining the magnitude of the differences between the two refractivity platforms appears to be related to the vertical gradient of refractivity, due to the difference in observation height between the radar and a surface station.

# 1. Introduction

Near-surface atmospheric refractivity was first retrieved using conventional weather radar by Fabry et al. (1997) and Fabry (2004) on McGill University's S-band radar. Since that innovation, radar refractivity experiments have been conducted in the Oklahoma Panhandle (Weckwerth et al. 2005; Fabry 2006; Wakimoto and Murphey 2009), northeast Colorado (Roberts et al. 2008), and southwest and central Oklahoma (Cheong et al. 2008; Heinselman et al. 2009; Bodine et al. 2010). Moreover, radar refractivity studies have become global, as the United Kingdom (Nicol et al. 2008) and France (Boudjabi and Parent du Châtelet 2008) are conducting radar refractivity experiments on operational magnetron radars. Many radar refractivity studies have found very high correlation between surface observations and radar refractivity, and observed differences were generally small (e.g., Fabry et al. 1997; Fabry 2004; Weckwerth et al. 2005).

One of the main goals of refractivity retrieval using weather radar is to observe atmospheric moisture with accuracy and resolution not attainable by any other observational platform in existence today. Studies by Fabry et al. (1997) and Fabry (2004) have shown how refractivity can be used to estimate low-level moisture due to its strong interdependence at warm temperatures. Radar refractivity has an effective resolution of approximately 4 km, and a temporal resolution of 4–10 min, depending on the radar scanning strategy and target density. Coincidentally, many studies have acknowledged that high-resolution observations of near-surface moisture fields may be the key to improving the accuracy in the prediction of convection initiation (e.g., Emanuel et al. 1995; Dabberdt and Schlatter 1996; National Research Council 1998). Several radar refractivity studies have shown that high-resolution refractivity data could potentially improve convection initiation nowcasting by identifying boundaries not observed in reflectivity (Weckwerth et al. 2005; Roberts

et al. 2008), and identifying areas of small-scale moistening unobserved by surface stations (Bodine et al. 2010). Wakimoto and Murphey (2009) showed that maxima of the total derivative of radar refractivity ( $DN/Dt$ ) tended to be collocated with cumulus development. While these studies have identified possible applications for forecasting, an operational evaluation of refractivity at the Norman, Oklahoma, Weather Forecast Office (WFO) determined that significant benefits were not obtained from using radar refractivity retrievals (Heinselman et al. 2009). Hence, future research should focus on determining new applications of refractivity data that provide new information to forecasters.

Although radar refractivity generally provides good agreement with surface observations, significant differences have been observed. Fabry (2004) found that radar refractivity retrievals generally agreed well with surface observations over a 60-day period. However, they noted that differences may occur if meteorological conditions at the surface and the target height become significantly different (e.g., during an inversion), resulting in fairly large differences (5 – 10 N-units in some cases) between the surface station and radar observations (cf. Fig. 8 in Fabry 2004). Weckwerth et al. (2005) found a high correlation between radar refractivity observations and surface mesonets, profilers, soundings, aircraft observations, and other observations. Similarly, they noted differences between surface and radar observations of refractivity, and suspected that the difference in height of clutter targets and surface observations caused these differences in observations. Moreover, the largest refractivity differences were found at higher relative humidities and higher latent heat fluxes.

The purpose of this study is to investigate sources of uncertainty associated with radar refractivity retrievals. To successfully use radar refractivity quantitatively, one must first understand the characteristics and magnitude of theoretical sources of uncertainty. This study examines over

two years of radar refractivity data to investigate many of these error sources, and determines the seasonal variability of radar refractivity differences. The study briefly reviews sources of error presented in previous studies, and then investigates errors due to magnetron frequency drift, and reference map representativeness. Errors due to magnetron frequency drift and reference map representativeness can be significant, and have not been thoroughly discussed. Then, the sampling inconsistencies between radar and surface observations (Fabry 2004; Weckwerth et al. 2005) are investigated, and a theory for these differences is proposed. This study examines data from a Mesonet site in Norman, Oklahoma, which includes thermodynamic measurements at both 2 and 9 m. These measurements provide an opportunity to directly compare low-level refractivity gradients to observed refractivity differences, and to examine errors associated with sampling inconsistencies.

Large errors in refractivity can have a major impact on quantitative studies, such as investigating the effects of assimilating radar refractivity into a numerical weather prediction (NWP) model for predicting convection initiation (Montmerle et al. 2002; Sun 2005; Gasperoni et al. 2009). These small inconsistencies in refractivity measurements can produce significant errors in the representation of moisture and temperature fields, and consequently, create unrealistic initial conditions and forecasts when assimilated into a NWP model. For instance, refractivity sampling error of several N-units is equivalent to a surface dew point temperature error on the order of 1–2°C. Refractivity errors of this magnitude can cause a substantial error in the thermodynamic profile of the lower troposphere, affecting the occurrence or absence of convection initiation (Crook 1996). While the potential utility of refractivity (and its relationship to atmospheric moisture) can be easily understood for purposes such as operational forecasting and numerical prediction of convection, a rigorous method of quantitatively validating radar refractivity has not been presented in the liter-

ature. This study has found significant refractivity differences at times, which would render radar refractivity useless for NWP model assimilation or for any other quantitative purpose. In response to this finding, a number of theoretical sources of refractivity differences and their potential impact were analyzed and are presented here.

This paper is organized as follows. Section 2 presents an overview of the radar refractivity algorithm, and the experimental design. In Section 3, a review of error sources is presented and some challenges to implementing radar refractivity operationally are discussed. Section 4 presents large refractivity differences between KTLX and several surface stations, and presents a theory for the observed mismatch. These refractivity differences are compared to 2- and 9-m surface observations of refractivity from the Oklahoma Mesonet. Conclusions and a discussion of the results follow in Section 5.

## 2. Radar refractivity experimental design

To perform the validation study, surface observations of refractivity ( $N$ ) were derived from data provided by the Oklahoma Climatological Survey’s Mesonet network (Brock et al. 1995; McPherson et al. 2007), using an equation defined by Bean and Dutton (1968):

$$N = 77.6 \frac{p}{T} + 3.73 \times 10^5 \frac{e}{T^2}, \quad (1)$$

where  $p$ ,  $T$ ,  $e$  are atmospheric pressure (hPa), temperature (K) and vapor pressure (hPa), respectively. The first and second terms of (1) are referred to as the “dry” ( $N_{dry}$ ) and “wet” ( $N_{wet}$ ) terms of refractivity, respectively. Vapor pressure is derived from the Mesonet using relative humidity and temperature measurements. The Mesonet provides measurements of the atmosphere at 5-min

intervals, providing refractivity measurements at a similar frequency to full volumetric scans of a conventional weather radar.

The radar refractivity algorithm used for klystron-based WSR-88D radars can be summarized by the following equation derived in Fabry et al. (1997), and using the convention for phase discussed in Cheong et al. (2008):

$$\Delta N = -10^6 \frac{c}{4\pi f} \frac{\partial}{\partial r} [\phi(r, t_1) - \phi(r, t_0)] = -10^6 [n(r, t_1) - n(r, t_0)], \quad (2)$$

where  $c$  is the speed of electromagnetic waves in a vacuum,  $f$  is the radar transmit frequency,  $\phi$  is the echo phase,  $n$  is the refractive index, and  $t_1$  and  $t_0$  are the observation and reference times, respectively. Absolute refractivity may then be determined by summing a reference field of refractivity, typically obtained from a smoothed field of surface refractivity observations at a reference time, to a field of refractivity change since  $t_0$ , defined in (2). The relation shown in (2) is of significant meteorological importance, because it provides a method of estimating atmospheric refractivity using data from operational weather radars. The refractivity algorithm used at in the present study (Cheong et al. 2008) produces a spatial resolution of approximately 4 km, which is similar to that presented by Weckwerth et al. (2005). The algorithm provides estimates of near-surface atmospheric moisture at temporal and spatial scales much finer than that of any *in situ* or remote sensing capability available today.

The current study also analyzes refractivity data derived from the magnetron-based CASA radar network in southwestern Oklahoma (McLaughlin et al. 2009). The frequency of a magnetron is dependent on temperature and is known to drift substantially over time. If the frequency drifts through a substantial portion of its bandwidth, it is typical to adjust a local oscillator to bring the intermediate frequency back to a desired value. When these corrections occur, the echo phase

is substantially altered; (2) cannot be used if a frequency correction has occurred between the reference time and a later radar scan time. The notion of using a reference time from prior days therefore does not apply when deriving refractivity from a magnetron-based radar.

To circumvent the effects of such a frequency correction, “scan-to-scan” refractivity change is utilized. Scan-to-scan refractivity is derived by substituting the previous radar scan’s phase field for the phase field from a reference time, providing a field of refractivity change occurring between two radar scans. If scan-to-scan refractivity were to be integrated through time, a field of refractivity change since the beginning of the integration would result. This integration can only be performed through a series of radar scans in which the transmitter frequency was not corrected. The use of phase data from every radar scan introduces increased uncertainty into  $\Delta N$  compared to that derived by (2) using a stable transmitter frequency, since each phase sample may contain some error. However, the long-term effects of integrating phase containing error are limited due to its random and zero-mean characteristics, producing little cumulative effect over time. As with the WSR-88D system, absolute refractivity  $N$  is derived by summing the integrated scan-to-scan refractivity to a smoothed background field of Mesonet refractivity obtained from the beginning of the scan-to-scan integration.

Fig. 1 shows the locations of the radars used for the present refractivity experiment, which include two WSR-88D radars, four CASA radars, and the Phased Array Radar (PAR; Cheong et al. 2008). Due to the operational usage of the WSR-88D systems, a nearly unbroken dataset of refractivity exists for KTLX and Frederick, Oklahoma (KFDR). This study focuses on KTLX because six Mesonet stations are located within good refractivity coverage. KFDR only has three Mesonet stations within 50 km, and only the Grandfield (GRAN) Mesonet station is located in suitable refractivity coverage for a valid comparison. The Tipton, Oklahoma (TIPT) Mesonet

station lies in a relative minima in elevation (about 370 m AGL) with higher terrain (400+ m AGL) closer to the radar, which appears to restrict clutter coverage. A small region of refractivity data exists near the Atlas, Oklahoma (ALTU) Mesonet site, however the refractivity data retrieved here tend to exhibit higher variability.

An example evolution of radar refractivity using KFDR is shown in Fig. 2. Many small-scale perturbations can be seen traversing the domain, with a sharp refractivity gradient moving east to west through the field between 0002 and 0045 UTC (1902 and 1945 local time [LT]) on the evening of 12 June 2009. This boundary is evidence of a retreating dryline. Drylines are easily seen using refractivity (e.g., Weckwerth et al. 2005) due to the sharp discontinuity in atmospheric moisture across its interface, and the strong dependence of refractivity on moisture at warmer temperatures (Fabry et al. 1997). Observations of atmospheric moisture related to an atmospheric phenomena, such as a dryline, at unprecedented resolution may be critical for a forecaster and a NWP model to properly assess the state of the atmosphere and improve prediction capabilities of future atmospheric processes, such as convection initiation.

The comparison between the radar and surface stations begins by determining the range and azimuth of the radar range gate coincident with each Mesonet station within the radar's refractivity domain. These individual gates may be masked during some periods by clutter quality control processing. To ensure temporal continuity and a rigorous long-term statistical comparison, a spatial median of radar refractivity is derived from a  $3 \times 5$  grid of range gates (in azimuth and range, respectively), centered on each Mesonet station. This radar refractivity estimate is compared to Mesonet refractivity observations. The areal coverage of the  $3 \times 5$  grid of gates is approximately  $700 \times 1000$  m at a range of 20 km from the radar.

To investigate the impact of changes in the vertical refractivity gradient on radar refractivity measurements, the Oklahoma Climatological Survey calibrated and installed new instrumentation at the 9-m height on the NRMN Mesonet tower. The new sensors at 9 m, calibrated with respect to similar instrumentation at 2 m, provided two observation levels of temperature, wind speed, and relative humidity. Vertical gradients of these variables, as well as many derived parameters, were calculated from this dataset to fully understand the stability of the near-surface atmosphere. Data collection from the newly installed instruments began 20 August 2009. In addition, the data logger at NRMN was updated to sample the atmosphere every minute at both the lower and upper instrumentation levels, a much higher frequency than previously available using standard 5-min Mesonet data.

Any differences between Mesonet and radar refractivity measurements are described by

$$\epsilon^i = N_{mesonet}^i - N_{radar}^i, \quad (3)$$

where  $\epsilon^i$  is the refractivity difference for the  $i$ th radar scan. The closest Mesonet observation to the scan time of the radar is used for comparison to each radar refractivity estimate. Using conventional Mesonet observations, the largest possible temporal difference between radar and Mesonet refractivity retrievals is 2.5 min; using data from the upgraded NRMN Mesonet tower, this maximum difference shrinks to 30 s. Since the PBL can change and evolve rapidly at any one location, the high-frequency NRMN refractivity observations ensure that the surface measurement is as temporally correlated as possible to any given radar scan. Since NRMN is located within the KTLX refractivity domain, and has the capability to observe the atmosphere rapidly at two levels, this study focuses on the relationship between refractivity samples taken by NRMN and KTLX. Observed refractivity differences are related to atmospheric processes observed from the NRMN

dataset.

To study the range of refractivity differences observed throughout the experiment, one-hour means of refractivity difference (4) were computed for each Mesonet station,  $n$ . The averaging helps mitigate the effects of noise or other short-term variations in refractivity differences. Then, the one-hour means for each Mesonet station,  $\overline{\epsilon}_n$ , were averaged to produce a mean radar refractivity difference for the radar,  $\overline{\epsilon}$ , as shown by (5). The number of Mesonet stations is given by  $N$ , and the number of volume scans is  $M$ .

$$\overline{\epsilon}_n = \frac{1}{M} \sum_{m=1}^M \epsilon_{m,n}^i \quad (4)$$

$$\overline{\epsilon} = \frac{1}{N} \sum_{n=1}^N \overline{\epsilon}_n \quad (5)$$

Then, the diurnal range of refractivity difference,  $R$ , was computed by taking the difference between the maximum one-hour mean refractivity difference,  $\overline{\epsilon}_{max}$ , and the minimum one-hour mean refractivity difference,  $\overline{\epsilon}_{min}$ , over one day.

$$R = \overline{\epsilon}_{max} - \overline{\epsilon}_{min} \quad (6)$$

Since Mesonet data at two levels were only available for part of the experiment, radiosonde data from Norman, Oklahoma (KOUN) were also examined. Vertical refractivity gradients were computed from KOUN radiosonde data. Radiosonde data at 0000 UTC were obtained for each day between February 2008 and April 2010. Given that the low-level refractivity gradients affecting refractivity measurements are confined to the surface layer, refractivity gradients were computed if sufficient data (at least two measurements) were available in the lowest 50 m. If two measurements were available in the lowest 50 m, surface layer refractivity gradients were computed.

### **3. Challenges for implementation of radar refractivity retrievals**

#### **3a. Review of refractivity error sources**

This section briefly reviews error sources discussed in previous studies, and Table 1 compares many of these error sources. Fabry (2004) presents a very thorough discussion of errors affecting refractivity measurements. He defines the intrinsic phase of a target as the component of the phase affected by a target's shape, range from the radar, and target illumination. Changes in the intrinsic phase of the target can result in errors in refractivity measurements. For example, vegetation sway or bending results in fluctuations of a target's range from the radar as the vegetation oscillates around or deviates from a central position, resulting in fluctuations in the target's phase. Fabry (2004) found that vegetation sway is one of the largest error sources, potentially biasing refractivity measurements by  $\pm 10$  N-units (for a single target). Anomalous propagation (AP) can affect the intrinsic phase of clutter targets by changing the apparent shape of the target, and changing the total path length to the target (Table 1). These errors are relatively small compared to vegetation sway. The target's intrinsic phase also varies as a result of precipitation in the resolution volume (random effect on phase), and coating of clutter targets with water or ice (Fabry 2004). Finally, variations in the height of clutter targets and changes in the vertical gradient of refractivity can increase the noise of phase measurements (Park and Fabry 2010).

Other errors can result from propagation delay or radar system changes. Propagation delay occurs as the electromagnetic wave slows down through water vapor or other media. Precipitation can introduce propagation delay (Fabry 2004), and may result in a relatively large bias in refractivity in very heavy precipitation because of the large propagation delay (Bodine et al. 2009).

However, clutter targets in heavy precipitation may be censored by quality control. Frequency drift can also impact radar refractivity measurements. During the Refractivity Experiment for H<sub>2</sub>O Research and Collaborative Operational Technology Transfer (REFRACTT; Roberts et al. 2008), they determined that the frequency drift of the klystron transmitter was less than 0.4 ppm, or a refractivity error of 0.4 N-units.

### **3b. Magnetron frequency drift**

While the stable frequency of klystron transmitter minimizes errors caused by frequency drift, magnetron transmitters have significant frequency drift. Determining the errors associated with transmitter frequency drift is important because current refractivity experiments around the world (e.g., Nicol et al. 2008; Boudjabi and Parent du Châtelet 2008) are made with magnetron radars. Refractivity errors associated with magnetron transmitters have not been examined, so a brief investigation is presented here using observations from the Cyril, Oklahoma (KCYR) CASA radar.

As stated earlier, magnetron frequency can drift as a function of temperature. The transmitter frequency of the CASA radars have been known to drift up to 500 kHz over a matter of a few hours, especially during start up. An analysis of a modified version of (2) shows that a frequency change of that magnitude can produce an error on the order of 10 N-units. An error this large is quite substantial, and must be corrected if accurate measurements of refractivity are to be extracted using magnetron-based radars. A simple solution would be to measure the transmit frequency, and to subtract any effects of frequency changes since the reference time  $t_0$ . Using a finite difference approximation for the range derivative in (2), the bias introduced by frequency changes can be

expressed as,

$$\Delta N = -\frac{10^6}{2\pi} \left( 1 - \frac{f_0}{f_1} \right), \quad (7)$$

where  $f_0$  and  $f_1$  are the frequencies at the reference and measurement times, respectively (Michaud 2010).

Fig. 3 is an example of refractivity change  $\Delta N$  since the reference time (set here to 0000 UTC [1900 LT]), as sampled by the Apache (APAC) Mesonet station and KCYR. Also provided in Fig. 3 is the KCYR refractivity change corrected for the observed transmitter frequency drift over the same time period. It can be seen that the refractivity correction in this case is generally on the order of 2 to 4 N-units, corresponding to an observed frequency drift of  $\pm 200$  kHz since 0000 UTC. The transmit frequency of the magnetron increases (decreases) with decreasing (increasing) internal system temperature since the reference time, inducing a negative (positive) refractivity change bias. In the example provided by Fig. 3, the internal temperature of KCYR decreased after 0000 UTC (near the time of sunset), requiring a positive correction to refractivity until 1500 UTC (1000 LT). At that time, the ambient air temperature was increasing rapidly (per APAC data), causing the radar's internal temperature to increase and requiring a negative correction throughout the rest of the day. If refractivity derived from magnetron-based radars, such as the CASA radars, is to be used quantitatively, then knowledge of the transmitter frequency at each radar scan and the amount of correction needed to remove any frequency drift effects is vital.

### **3c. Reference map representativeness**

To reduce phase wrapping, radar refractivity requires two sets of phase measurements. One set of phase measurements is made at a reference or calibration time, and the second set is made

at the desired measurement time (Fabry 2004). Fabry (2004) outlines a procedure for making a reference set of phase measurements (hereafter, called the reference map). In his study, Fabry recommended producing reference maps when refractivity is horizontally and temporally homogeneous, often under windy and cool conditions following stratiform precipitation. Accordingly, a single value of refractivity is assumed to be valid everywhere at the reference time ( $N=N_{ref}$ ). In central Oklahoma, however, moisture gradients are rarely small enough to assume a constant value of refractivity. Thus, Oklahoma Mesonet data are interpolated to produce reference refractivity values (Cheong et al. 2008).

The validity of (2) and the reference map requires that the field of suitable clutter targets for radar refractivity retrieval are identical at both the reference time and some future observation time, and that changes in echo phase from these targets are due entirely to changes in atmospheric refractivity. As described in Section 3a, a clutter target's phase may change due to vegetation sway, or more generally due to changes in a target's shape (e.g., changes in foliage, damage, construction). If the clutter field itself changes, then the integration of echo power returned from clutter targets produces a change in echo phase which is not related to a change in atmospheric conditions. If the character of the clutter field changes, then a new, more representative reference phase field must be created.

To address the need for an improved method of selecting reference maps, a semi-automated method of reference map production was created. The semi-automated method searches a time series of Oklahoma Mesonet data within the refractivity domain (Fig. 1) for the following conditions:

1. Rainfall rate  $R < 0.01 \text{ mm hr}^{-1}$
2. Wind speeds  $|\vec{u}| < 5 \text{ m s}^{-1}$

3. Refractivity range  $\overline{N_{max} - N_{min}} < 5$  N-units.

The conditions must be observed for a minimum of 10 consecutive radar scans to ensure temporal consistency, and mean rainfall rate and wind speeds must remain below the aforementioned thresholds. The refractivity range, or the mean difference between the highest ( $N_{max}$ ) and lowest ( $N_{min}$ ) refractivity values, must be below 5 N-units for at least 10 consecutive radar scans.

Once the criteria have been met, reference maps are produced for the periods that met the criteria above, and a series of additional quality checks are performed to ensure a quality reference map. Even if reference maps are produced under these conditions, poor reference maps can still result owing to variations in clutter coverage at different reference map times. Thus, fields of the reliability index (RI; Fabry 2004), Mesonet refractivity, and phase are further examined by researchers to determine which reference maps provide the best clutter coverage and the smallest gradients in Mesonet refractivity. This quality check process could be automated by setting a threshold for the RI, and selecting the reference map with the highest number of gates exceeding the RI threshold.

Based on the semi-automated algorithm described above, reference maps were produced at six different times on 12 July 2009. Fig. 4 presents the refractivity measurements using the six different reference maps, and reveals that reference maps produced at different times can yield large biases in refractivity measurements. The reference maps are clustered into two groups: reference maps made between 0400 – 1600 UTC and reference maps made between 2000 – 0100 UTC. These two groups exhibit a nearly constant offset or “shift” of about 7 N-units. This offset could result from different vertical refractivity gradients when the reference maps were produced, which would explain the clustering. As will be discussed in Section 4, a diurnal variation in the vertical

refractivity gradient is observed which may explain the reference map “shift”. Fig. 5(a) presents a two-month time series of the radar refractivity difference (3), which is discussed in greater detail in the forthcoming section. However, examining the radar refractivity difference on 12 July 2009, the diurnal range of radar refractivity differences is approximately 9 N-units, close to the maximum “shift” observed in the reference maps. Moreover, the reference maps made between 0400 – 1600 UTC were produced during relatively small refractivity differences whereas the 2000 – 0100 UTC were produced during larger (more negative) refractivity differences.

If reference maps are made at different times when vertical refractivity gradients are different, refractivity values will be shifted at subsequent measurement times. Table 2 shows examples of how vertical refractivity gradients affect refractivity measurements for different target heights. In both examples, it is assumed that the 2-m surface refractivity does not change. The vertical refractivity gradient at the reference time,  $t_0$ , is  $-0.1$  and  $-0.5$  N-units  $m^{-1}$  for each case, hereafter called the small vertical gradient and large vertical gradient cases, respectively. At the reference time, even though the radar is sampling a height above 2 m, the refractivity measurement is set equal to the 2-m refractivity observation. As the vertical refractivity gradient changes at later measurement times ( $t_1$  and  $t_2$ ), the measured radar refractivity value changes even though the 2-m measurement remains unchanged, resulting in large differences between the radar and surface observation. At time  $t_2$  with a vertical refractivity gradient of  $-1$  N-unit  $m^{-1}$ , radar refractivity values for the small and large vertical gradient reference maps are 283.8 and 291 N-units, respectively (bolded text in Table 2). In Section 4, diurnal changes in vertical refractivity gradients will be investigated in more detail.

In this study, tradeoffs have been observed in producing reference maps. First, clutter targets may sway under windy conditions, but may remain stationary under calm conditions. If

a reference map is made under windy conditions, clutter targets that may be usable under calm conditions are censored. Thus, reference maps made during relatively calm conditions should maximize refractivity coverage. Adaptive clutter censoring (e.g., quality index discussed in Fabry 2004; Cheong et al. 2008), however, is required to ensure that clutter targets are censored when vegetation sway or target motion becomes a problem under windy conditions. In the present study, creating reference maps under relatively calm conditions provide increased refractivity coverage for KTLX because the southeastern part of the domain is dominated by vegetation.

A second tradeoff involves producing reference maps under different propagation conditions. More clutter targets are illuminated during superrefraction compared to subrefraction (e.g., well-mixed conditions), hence increasing refractivity coverage. However, producing reference maps during a period of large vertical refractivity gradients will increase errors due to sampling inconsistencies (Fabry 2004; Weckwerth et al. 2005) and increase the phase variance due to target height variance (Park and Fabry 2010).

The reference map remains an important, but poorly understood component of radar refractivity retrieval. Future research should investigate how to maximize radar refractivity coverage while minimizing differences introduced by changes in vertical refractivity gradients, and should develop a fully automated method of reference map production. For this study, new reference maps were created every 3 – 4 months because data quality degraded over longer time periods and aliasing occurred frequently as refractivity values changed significantly seasonally. If refractivity were implemented on the WSR-88D network, over 150 radars would need reference maps as frequently as every 3 – 4 months. For a CASA network of radar refractivity, tens of thousands of radars could need reference maps. Hence, implementing radar refractivity in an operational radar network likely requires automated reference map production. If a future operational radar network

with multiple frequencies were implemented, refractivity retrieval might be possible without using a reference map (Cheong and Palmer 2009).

## **4. Sampling inconsistencies**

The height of radar refractivity measurements is unknown because the mean clutter height and beam propagation are unknown (a mean height based on the integrated power from the beam illuminating the target). The height of clutter targets is, however, generally much higher than surface measurements (e.g., Mesonet at 2 m), so surface and radar refractivity measurements are measuring different heights of the atmosphere. Fabry (2004) explains how the radar observes atmospheric refractivity several tens of meters AGL due to the height of the clutter targets used, and that vertical gradients of refractivity near the surface could cause significant discrepancies between radar and surface observations of refractivity. Weckwerth et al. (2005) found only small changes in refractivity with respect to height throughout the lowest several hundred meters of the atmosphere. However, that study was performed in the Oklahoma Panhandle, where conditions are typically much drier than in central Oklahoma. In this section, the hypothesis that the existence of large vertical refractivity gradients could explain the larger refractivity differences is investigated using KTLX and Mesonet data over a two-year period. In this section, the hypothesis that the existence of large vertical refractivity gradients could explain the larger refractivity differences is investigated using KTLX and Mesonet data over a two-year period.

#### 4a. *Surface layer refractivity gradients*

A diurnal evolution of vertical moisture and temperature gradients is observed in the surface layer. In the unstable, afternoon surface layer, large surface moisture fluxes result in decreasing moisture as a function of height (e.g., Stull 1988). Large, negative moisture gradients are found near the surface transitioning to small moisture gradients at the top of the surface layer (Stull 1988). Large, negative vertical temperature gradients also characterize the afternoon surface layer, and temperature gradients are often superadiabatic. Leading up to sunset, the surface layer undergoes the early evening transition (EET; Acevedo and Fitzjarrald 2001). The EET is characterized by a developing stable surface layer, reduced mixing, and often an increase in moisture. The moisture increase results from increased evaporation, which is “trapped” by the stable surface layer (Fitzjarrald and Lala 1989). Hence, vertical moisture gradients may result during the EET due to increases in moisture at the surface. Temperature inversions arise in the stable surface layer, owing to rapid cooling of the surface.

The impact of these vertical moisture and temperature gradients on refractivity varies seasonally because refractivity is more sensitive to moisture at warmer temperatures (1). Hence, in the warm season, refractivity is more sensitive to moisture than temperature, so the vertical refractivity gradients are dominated by vertical moisture gradients. Fig. 6 presents a monthly climatology of the mean surface layer refractivity difference between 2 and 9 m from the NRMN Mesonet site between September 2009 and May 2010 (9-m data unavailable prior to 20 August 2009). During the warm season (e.g., 09/09 or 05/10), large vertical refractivity gradients (exceeding 0.4 N-units  $\text{m}^{-1}$ ) are observed in the late afternoon resulting from sharp moisture decreases as a function of height. In individual cases, vertical refractivity gradients as large as 1 or 2 N-units  $\text{m}^{-1}$  are ob-

served. During the EET, a secondary maximum in vertical refractivity gradients is observed (e.g., 05/10), probably attributed to increased evaporation. In the cool season, much smaller refractivity gradients are observed in the afternoon because refractivity is less sensitive to moisture. Large vertical refractivity gradients form overnight owing to strong nocturnal inversions (e.g., 01/10), resulting in vertical refractivity gradients of above  $0.2 \text{ N-units m}^{-1}$ .

#### **4b.** *Refractivity difference case studies*

A very large diurnal range of differences between radar refractivity measurements and the Mesonet are observed at times during the radar refractivity experiment, sometimes exceeding 30 N-units over 24 h. As discussed in Section 3c, the reference map choice can “shift” refractivity measurements. Hence, since the actual value of refractivity can be shifted by using a different reference map, the range of refractivity differences is more important than the refractivity difference value. In the forthcoming case studies, radar refractivity differences are compared to the 2-9 m refractivity difference and Richardson number. The 2-9 m difference is shown for periods after 20 Aug 2009 when 9-m Mesonet moisture measurements were available for NRMN.

**i. 18 June – 08 August 2009** Very large radar refractivity differences are often observed in the summer. Fig. 5a presents a time series of radar refractivity differences computed for six Mesonet stations within good clutter coverage between 18 June – 08 August 2009. The diurnal range of refractivity difference sometimes exceeds 30 N-units (e.g., 19 July 2009). All of the Mesonet stations exhibit a prominent diurnal trend, which suggests that the cause of these refractivity differences affects the entire domain fairly similarly. However, the individual Mesonet stations can disagree

for brief periods, which could result from differences in target height among stations or differences in the spatial scales of sampling for the Mesonet and the radar. The Spencer, Oklahoma (SPEN) Mesonet station in particular often exhibits significant disagreement with the radar measurements, which could also be related to relatively poor clutter coverage in the area. Mean values of radar refractivity difference were computed for each surface station between 18 June – 08 August 2009, but the differences in mean values among stations were quite small compared to the variance. So, the differences between stations were not statistically significant.

During the summer, the radar refractivity difference time series reveals a diurnal trend similar to the observed low-level refractivity gradients observed by the Mesonet, suggesting that the sampling differences may be related to the magnitude of low-level refractivity gradients (Figs. 5a,6). The radar refractivity difference generally decreases after sunrise, and can decrease very rapidly (e.g., 19 July 2009), or decrease more gradually (e.g., 14 July 2009 in Fig. 5a). In some cases, the decrease in radar refractivity difference occurs later in the afternoon (e.g., 08 – 11 August 2009 in Fig. 5a) after remaining relatively constant throughout the morning and afternoon. Just before sunset (2200 – 0000 UTC), the radar refractivity differences generally increase as the surface stable layer begins. After sunset, the highest radar refractivity differences are typically observed, and differences remain relatively constant overnight.

Stability appears to play a role in determining the magnitude of radar refractivity differences. On days when stable conditions persist overnight (indicated by black circles on Fig. 5a) and unstable conditions persist during the afternoon (indicated by red circles on Fig. 5a), a larger range of radar refractivity difference ensues (e.g., 23 – 29 June 2009 in Fig. 5a). Moreover, the transition from stable to unstable conditions in the morning results in decreasing radar refractivity differences, and the transition from unstable to stable conditions in the evening coincides with

increasing radar refractivity differences. When neutral stability prevails, smaller radar refractivity differences occur and a smaller diurnal range of radar refractivity differences is typically observed. While Mesonet observations showed large refractivity gradients between 2 and 9 m in the late afternoon, such large refractivity gradients may not be representative of through the entire surface layer or the vertical depth of clutter targets. Latent heat fluxes are large near the surface, producing strong vertical moisture gradients whereas moisture gradients near the top of the surface layer are near zero owing to well-mixed conditions (Stull 1988). In the stable surface layer, however, large gradients of temperature and sometimes moisture are observed over a deeper layer. Thus, the large refractivity gradients observed by the Mesonet in the early evening may be more representative of refractivity differences observed over a deeper layer characteristic of refractivity measurements. Hence, the large vertical gradients sustained overnight may result in larger refractivity gradients, explaining the maximum in refractivity differences overnight.

To determine periodicities characterizing the radar refractivity difference, a periodogram was computed for the radar refractivity difference for each station (Fig. 5b). The periodogram for each station reveals a clear peak at a frequency of  $1 \text{ day}^{-1}$ , confirming that the diurnal trend in radar refractivity difference is a common feature in the radar refractivity time series for each station (same trend for SPEN and OKCW, but not shown). While the periodogram revealed a peak at a frequency of  $1 \text{ day}^{-1}$ , the radar refractivity differences do not always exhibit a diurnal trend (e.g., 07 July or 21 July 2009). Examining higher frequencies, no clear peaks are observed consistently at multiple Mesonet stations. Although frequencies less than  $1 \text{ day}^{-1}$  are observed in the time series, the transition time between higher and lower refractivity differences varies substantially and occurs at different times of day (e.g., varies in part due to sunrise or sunset times), so the periodogram lacks a prominent peak at higher frequencies.

**ii. 20 August – 10 October 2009** In the late summer and early fall, a less prominent diurnal trend occurs, and the diurnal range of refractivity differences are smaller (Figs. 7, 8). Between 02–04 September 2009, the time series of radar refractivity difference shows small diurnal ranges of refractivity differences. However, large refractivity differences can still occur, as observed on 29 September 2009 when the diurnal range of refractivity exceeds 25 N-units. For this particular case, large refractivity differences occurred overnight under high pressure and stable conditions (Fig. 8).

Correlation coefficients were computed between the radar and the 2-m Mesonet refractivity measurements ( $r_{NRMN-2m}$ ) and the radar and 9-m Mesonet refractivity measurements ( $r_{NRMN-9m}$ ). Between 20 Aug – 16 September 2009, the 99% confidence interval for  $r_{NRMN-2m}$  is 0.922 – 0.932 and the 99% confidence interval for  $r_{NRMN-9m}$  is 0.935 – 0.944 (Fig. 7). Although the differences in the correlation coefficients are small, the confidence interval shows statistically significant differences between the correlation coefficients of the two time series. Thus, the 9-m observations show better correlation compared to the 2-m observations. Given that the mean target height is likely much higher than 2 m, the higher correlation at 9 m is not surprising. Higher correlations might be expected if higher observations were available.

Between 16 September – 09 October 2009, even higher correlations are observed at both 2 and 9 m (Fig. 8). The confidence interval for  $r_{NRMN-2m}$  is 0.966 – 0.971 and the 99% confidence interval for  $r_{NRMN-9m}$  is 0.974 – 0.978. As observed during the previous period, the 9-m Mesonet site exhibits higher correlation than the 2-m Mesonet site, indicating smaller differences in sampling inconsistencies at 9 m compared to 2 m.

In general, the radar refractivity differences correlate well with the 2–9 m refractivity dif-

ference, indicating that low-level refractivity gradients affect the observed refractivity differences. The correlation between the radar refractivity differences and 2–9 m refractivity differences is higher in the later period (Fig. 8), possibly because larger refractivity differences and coincident Mesonet vertical refractivity gradients are observed compared to the first period. Overall, the 2–9 m differences are smaller than the radar refractivity differences observed (approximately by a factor of 2 or 3), which also suggests that the target heights exceed 9 m.

**iii. 19 November – 13 December 2009** In the cool season, the time series between 19 November – 13 December 2009 reveals much smaller radar refractivity differences (Fig. 9), which only occasionally exceed  $\pm 10$  N-units. Radar refractivity differences between 05 – 10 December 2009 are quite small (generally  $\pm 2$  N-units), resulting from primarily neutral stability and very small surface layer gradients in moisture. Overall, radar refractivity differences for each Mesonet station exhibit better agreement with each other compared to the warm season.

The time series of the radar and the 2-m Mesonet observations, and the radar and 9-m Mesonet observations exhibit very high correlation. The confidence interval for  $r_{NRMN-2m}$  is 0.957 – 0.964 and the 99% confidence interval for  $r_{NRMN-9m}$  is 0.973 – 0.977. Hence, the 9-m observations show higher correlation than the 2-m observations, consistent with the trends observed during the warm season. The range of 2–9 m differences is slightly smaller than the range of radar refractivity differences observed. The smaller differences between these two time series could have two explanations. First, smaller differences could result if the mean (beam-weighted) target height decreased, possibly owing to increased refraction and more power illuminating the lower portions of clutter targets. Hence, the representative height of refractivity measurements would be lower and smaller sampling differences would result. Another explanation for the re-

duced differences between the two time series is that the vertical refractivity gradients above 9 m are relatively small compared to the warm season.

#### **4c.** *Climatology of refractivity differences*

The previous case studies show that radar refractivity differences exhibit a prominent diurnal trend, and the diurnal range of refractivity differences sometimes exceeds 30 N-units. To further characterize this diurnal trend and examine the seasonal characteristics of refractivity differences, the diurnal range of radar refractivity difference (described in Section 2) was computed for KTLX from March 2008 – April 2010 (Table 3). Fig. 10 presents histograms of the diurnal range of refractivity differences for 2009. The highest median diurnal range occur during the warm season, with the median diurnal range exceeding 8 N-units between May and August and the diurnal range exceeds 20 N-units on 17% of days. During July 2009, the median diurnal range is 11.8 N-units and exceeded 20 N-units on 24% of days. In the cool season, the median diurnal range is much lower, below 6 N-units between October and March. Very large diurnal ranges are uncommon, and only exceed 20 N-units when strong inversions are present (e.g., after a cold front passage).

The range of radar refractivity differences from 2008 and 2010 reveal similar trends to 2009 (Table 3). The median diurnal range of radar refractivity differences in the warm season are higher than the cool season. Moreover, the largest median diurnal range of refractivity differences corresponds to periods with higher surface layer refractivity gradients in the lowest 50 m, computed from KOUN radiosonde observations (Table 4). These data confirm the seasonal variability of radar refractivity differences presented in the preceding case studies.

#### **4d. Theory of radar refractivity differences caused by vertical refractivity gradient changes**

In Section 3c, an example of how different vertical gradients affect radar refractivity measurements was presented in Table 2. This example also illustrates how vertical refractivity gradients can cause large refractivity differences between a surface station and the radar. The change in vertical refractivity gradient between the reference and the measurement time introduces differences between refractivity measurements from a surface station and the radar. In the small ( $\frac{dN}{dz}$ ) gradient example for 20-m targets, radar refractivity differences of 7.2 and 16.2 N-units result from vertical refractivity gradients of -0.5 and -1 N-units  $m^{-1}$  (italicized text in Table 2). In the large ( $\frac{dN}{dz}$ ) gradient example for 20-m targets, radar refractivity differences of -7.2 and 9 N-units result from vertical gradients of -0.1 and -1 N-units  $m^{-1}$  (bold, italicized text in Table 2). In general, the magnitude of these differences increases as the target height increases, and as the difference between the vertical refractivity gradient at the reference and measurement times increases.

## **5. Conclusions and discussion**

This study investigated challenges for implementing radar refractivity retrievals on an operational network, including magnetron frequency drift, reference map issues, and sampling inconsistencies. Although magnetron frequency drift is known to affect refractivity measurements, the magnitude of these errors had not been measured previously. This study found that magnetron frequency drift can result in errors up to 10 N-units. To address the difficulties in producing reference maps, a semi-automated procedure for making reference maps was outlined. The study found that reference maps made at different times of day create a constant offset or “shift” of refractivity

values. A theory explaining how changes in vertical refractivity gradients can produce a “shift” of refractivity values is presented.

This study addressed the need for a thorough, quantitative investigation of radar refractivity differences, and utilized refractivity data from over 2 years (previous studies examined 90 days or less of data). Fabry (2004) and Weckwerth et al. (2005) suggested that radar refractivity differences may result from sampling differences resulting from changes in the vertical gradient of refractivity over time. This study investigated this hypothesis using Mesonet observations of moisture at 2 and 9 m, providing direct comparisons of surface layer refractivity gradients to refractivity observations.

Very large refractivity differences were observed during a two-year period of refractivity and Mesonet comparisons, much larger than refractivity differences found in previous studies (e.g., Fabry 2004; Weckwerth et al. 2005). Refractivity differences sometimes varied over 30 N-units in one day, and resulted from sampling inconsistencies between the two measurements. The greatest diurnal variations in radar refractivity differences occurred when persistent stable conditions were observed overnight, and persistent unstable conditions were observed during the afternoon. During both the warm and cool season, radar refractivity data exhibited higher correlation with 9-m Mesonet refractivity than 2-m Mesonet refractivity, indicating that the representative height of refractivity measurements was at least 9 m. Moreover, radar refractivity exhibited poorer correlation with 2-m and 9-m Mesonet observations during the warm season, suggesting that 2 and 9 m moisture measurements are less representative of refractivity measurements during the warm season.

Over the two-year period, the diurnal range of refractivity differences exhibited a prominent

seasonal trend. Radar refractivity differences are greater by nearly a factor of 2 in the warm season compared to the cool season, with median diurnal refractivity ranges exceeding 8 N-units during the warm season. The frequency of days with very large diurnal ranges of refractivity differences was also higher in the warm season. The higher sensitivity to moisture during the warm season, and larger vertical gradients of moisture may explain the larger diurnal range of refractivity differences in the warm season.

The results from this study have important implications for using refractivity data in forecasting and data assimilation applications. The reference map “shift” and large refractivity differences can significantly affect refractivity estimates. Given that one of the primary benefits of radar refractivity measurements are convection initiation forecasting in the warm season, the large diurnal range of refractivity differences poses a potentially significant problem for refractivity retrieval. For data assimilation, the “shift” and refractivity differences must be “corrected” to the surface, or refractivity data must be assimilated at the representative height of refractivity measurements. Unfortunately, the height of clutter targets is unknown and likely varies spatially and perhaps seasonally. Hence, methods to determine the height of the mean height of clutter targets or refractivity measurements should be developed, if possible. If refractivity data are assimilated with refractivity differences as large as 30 N-units, very unrealistic initial conditions will ensue.

For forecasting applications, the reference map “shift” and large refractivity differences may have smaller impacts when examining moisture gradients or scan-to-scan refractivity. For example, for boundary detection, a forecaster could examine refractivity to observe moisture gradients or scan-to-scan refractivity to observe temporal moisture changes (e.g., Weckwerth et al. 2005; Roberts et al. 2008; Heinselman et al. 2009). If vertical gradients of refractivity are relatively spatially homogeneous (certainly true compared to diurnal changes), then the sampling

inconsistencies affect the refractivity field homogeneously, and accurate measurements of horizontal gradients of refractivity are still obtained. Moreover, because scan-to-scan refractivity takes a phase difference over one volume scan, the vertical refractivity gradient changes over this period are probably quite small (except during the EET or just after sunrise). Hence, scan-to-scan refractivity may be immune to the problems caused by sampling inconsistencies. Although numerous challenges exist with refractivity retrieval using radar, the potential impact of high-resolution moisture measurements is great. So, research efforts focusing on minimizing these errors and discovering new applications of refractivity data should be pursued.

**Acknowledgments** Funding for this research was provided by the National Science Foundation through grant number ATM0750790. The first author was supported by an American Meteorological Society Fellowship. The authors would like to acknowledge the Oklahoma Climatological Survey for their work in providing Mesonet datasets, and for customizing the NRMN tower to the needs of the experiment. The authors also thank the Radar Operations Center for their work in providing data from KTLX and KFDR throughout this project. This work was partially supported by the Engineering Research Centers Program of the National Science Foundation under NSF Award 0313747. Any opinions, findings, conclusions, or recommendations expressed in this material are those of the authors and do not necessarily reflect those of the National Science Foundation. The authors also thank Tian-You Yu, Richard Doviak, and Dusan Zrnić for their input during project meetings. The authors also appreciate helpful discussions with Conrad Ziegler about surface layer observations.

## References

- Acevedo, O. C. and D. R. Fitzjarrald, 2001: The early evening surface-layer transition. *J. Atmos. Sci.*, **58**, 2650–2667.
- Bean, B. R. and E. J. Dutton, 1968: *Radio Meteorology*. Dover Publications, 435 pp.
- Bodine, D., P. L. Heinselman, B. L. Cheong, R. D. Palmer, and D. Michaud, 2010: A case study on the impact of moisture variability on convection initiation using radar refractivity retrievals. *J. Appl. Meteorol.*, **49** (8), 1766–1778.
- Bodine, D., R. D. Palmer, B. L. Cheong, P. L. Heinselman, D. S. Michaud, and G. Zhang, 2009: Can high-resolution surface moisture fields be retrieved in supercells? *34th Conf. on Radar Meteorology*, Amer. Meteor. Soc., Ed., Williamsburg, VA.
- Boudjabi, C. and J. Parent du Châtelet, 2008: Validation of refractivity measurements with magnetron transmitter radar. *Proceedings of the Fifth European Conf. on Radar Meteor. and Hydrology*, Helsinki.
- Brock, F. V., K. C. Crawford, R. L. Elliott, G. W. Cuperus, S. J. Stadler, H. L. Johnson, and M. D. Eilts, 1995: The Oklahoma Mesonet: A technical overview. *J. Atmos. Oceanic Technol.*, **12**, 5–19.
- Cheong, B. L. and R. D. Palmer, 2009: Single-scan radar refractivity retrieval: theory and simulations. *34th Conf. on Radar Meteorology*, Amer. Meteor. Soc., Ed., Williamsburg, VA.
- Cheong, B. L., R. D. Palmer, C. D. Curtis, T.-Y. Yu, D. S. Zrnić, and D. Forsyth, 2008: Refractivity retrieval using the Phased Array Radar: First results and potential for multi-function operation. *IEEE Tran. Geosci. Remote Sensi.*, **46**, 2527–2537.

- Crook, N. A., 1996: Sensitivity of moist convection forced by boundary layer processes to low-level thermodynamic fields. *Mon. Wea. Rev.*, **124**, 1767–1785.
- Dabberdt, W. F. and T. W. Schlatter, 1996: Research opportunities from emerging atmospheric observing and modeling capabilities. *Bull. Amer. Meteor. Sci.*, **77**, 305–323.
- Emanuel, K., et al., 1995: Report of first prospectus development team of the U.S. Weather Research Program to NOAA and the NSF. *Bull. Amer. Meteor. Sci.*, **76**, 1194–1208.
- Fabry, F., 2004: Meteorological value of ground target measurements by radar. *J. Atmos. Oceanic Technol.*, **21**, 560–573.
- Fabry, F., 2006: The spatial variability of moisture in the boundary layer and its effect on convective initiation: Project-long characterization. *Mon. Wea. Rev.*, **134**, 79–91.
- Fabry, F., C. Frush, I. Zawadzki, and A. Kilambi, 1997: On the extraction of near-surface index of refraction using radar phase measurements from ground targets. *J. Atmos. Oceanic Technol.*, **14**, 978–987.
- Fitzjarrald, D. R. and G. G. Lala, 1989: Hudson Valley fog environments. *J. Appl. Meteor.*, **28**, 1303–1328.
- Gasperoni, N. A., M. Xue, R. D. Palmer, J. Gao, B. L. Cheong, and D. S. Michaud, 2009: Low-level moisture analysis from refractivity data derived from a network of S-band and X-band radars using ARPS 3DVAR. *34th Conf. on Radar Meteorology*, Amer. Meteor. Soc., Ed., Williamsburg, VA.
- Heinselman, P. L., B. L. Cheong, R. D. Palmer, D. Bodine, and K. Hondl, 2009: Radar refractivity

- retrievals in Oklahoma: Insights into operational benefits and limitations. *Wea. Forecasting*, **24**, 1345–1361.
- McLaughlin, D., et al., 2009: Short-wavelength technology and the potential for distributed networks of small radar systems. *Bull. Amer. Meteor. Sci.*, **90**, 1797–1817.
- McPherson, R. A., et al., 2007: Statewide monitoring of the mesoscale environment: A technical update on the Oklahoma Mesonet. *J. Atmos. Oceanic Technol.*, **24**, 301–321.
- Michaud, D. S., 2010: Validation of radar estimation of low-level moisture fields using refractivity retrieval statistical analysis. M.S. thesis, University of Oklahoma, School of Meteorology, pp. 127.
- Montmerle, T., A. Caya, and I. Zawadzki, 2002: Short-term numerical forecasting of a shallow storms complex using bistatic and single-Doppler radar data. *Wea. Forecasting*, **17**, 1211–1225.
- National Research Council, 1998: *The Atmospheric Sciences: Entering the Twenty-First Century*. National Academy Press, pp. 373.
- Nicol, J., T. Darlington, A. Illingworth, K. Bartholemew, M. Kitchen, and E. Delaygue, 2008: Operational testing of radar refractivity retrieval for the UK radar network. *Proceedings of the Fifth European Conf. on Radar Meteor. and Hydrology*, Helsinki.
- Park, S. and F. Fabry, 2010: Simulation and interpretation of the phase data used by the radar refractivity retrieval algorithm. *J. Atmos. Ocean. Tech.*, **27**, 1286–1301.
- Roberts, R. D., et al., 2008: REFRACTT-2006: Real-time retrieval of high-resolution low-level moisture fields from operational NEXRAD and research radars. *Bull. Amer. Meteor. Sci.*, **89**, 1535–1548.

Stull, R. B., 1988: *An Introduction to Boundary Layer Meteorology*. Kluwer Academic, 666 pp.

Sun, J., 2005: Convective-scale assimilation of radar data: Progress and challenges. *Quart. J. Roy. Meteor. Soc.*, **131**, 3439–3463.

Wakimoto, R. M. and H. V. Murphey, 2009: Analysis of a dryline during IHOP: Implications for convection initiation. *Mon. Wea. Rev.*, **137**, 912–936.

Weckwerth, T. M., C. R. Pettet, F. Fabry, S. Park, M. A. LeMone, and J. W. Wilson, 2005: Radar refractivity retrieval: Validation and application to short-term forecasting. *J. Appl. Meteorol.*, **44**, 285–300.

## Figure Captions

- 1 A map of radars used for refractivity retrieval in central and southwestern Oklahoma. Refractivity domains are colored based on radar type: WSR-88D (red), CASA (blue), and PAR (black). Oklahoma Mesonet stations are labeled in brown and shown by the brown triangles. . . . . 39
- 2 A two-hour evolution of radar refractivity fields, using KFDR in southwest Oklahoma. Radar scans were taken every 4–5 min during this time period; for brevity, scans at 15-min intervals are shown. Notice the rapid return of much higher refractivity from the east after 0000 UTC (1900 LT). The locations of the Altus (ALTU), Tipton (TIPT), and Grandfield (GRAN) Mesonet stations are demarcated by the black triangles. . . . . 40
- 3 A comparison of sampled refractivity change, as derived from KCYR and the 2-m measurements from APAC, including frequency drift-corrected KCYR refractivity change. Refractivity difference is small during this period, with much of the difference being removed when correcting the data for the drift of the radar transmitter frequency. . . . . 41

- 4 A time series comparison of the radar refractivity difference between the 2-m Norman Mesonet and radar refractivity, computed for six different reference maps. The reference maps were created at six different times on 12 July 2009, and the time series shown is on 12 July 2009. The reference maps are clustered into two separate groups based on the time of day. The reference maps made overnight and during the morning (0400 – 1600 UTC), and reference maps made in the afternoon and early evening (2000 – 0000 UTC) are clustered. The reference map can “shift” refractivity estimates as much as 7 N-units depending on the choice of reference map. . . . . 42
- 5 a) Time series of radar refractivity difference for six Mesonet stations, showing the difference between the 2-m Mesonet and radar refractivity between 18 Jun – 13 Aug 2009, and b) periodogram of radar refractivity difference between 18 Jun – 13 Aug 2009. The time series reveals a prominent diurnal periodicity in radar refractivity difference. At the top of the time series plot, black circles indicate stable conditions with  $Ri > 0.25$  and red circles indicate unstable conditions with  $Ri < -1$ . When a large diurnal range of radar refractivity difference occurs, the surface layer is stable at night and very unstable during the afternoon. In the periodogram, a prominent peak is observed at a frequency of  $1 \text{ day}^{-1}$  for each Mesonet station. . . . . 43

6	Climatology of the hourly mean refractivity difference between 2 and 9 m from the NRMN Mesonet site (difference in N-units). The plots show the monthly hourly mean from Sep 2009 to May 2010. Larger refractivity differences are observed in the warm season (e.g., 09/09 or 05/10), particularly in the late afternoon. In the cool season, the largest refractivity differences are observed overnight, owing to strong nocturnal inversions and increased dependence of refractivity on temperature (e.g., 01/10). . . . .	44
7	Time series of radar refractivity difference for six Mesonet stations, showing the difference between the 2-m Mesonet and radar refractivity between 20 Aug – 15 Sep 2009. At the top of the time series plot, black circles indicate stable conditions with $Ri > 0.25$ and red circles indicate unstable conditions with $Ri < -1$ . The green horizontal line is plotted to show $Ri=0.25$ . . . . .	45
8	Time series of radar refractivity difference for six Mesonet stations, showing the difference between the 2-m Mesonet and radar refractivity between 16 Sep – 09 Oct 2009. At the top of the time series plot, black circles indicate stable conditions with $Ri > 0.25$ and red circles indicate unstable conditions with $Ri < -1$ . The green horizontal line is plotted to show $Ri=0.25$ . . . . .	46

- 9 Time series of radar refractivity difference for six Mesonet stations, showing the difference between the 2-m Mesonet and radar refractivity between 19 Nov – 13 Dec 2009. In general, radar refractivity differences are much smaller in the cool season compared to the warm season, with radar refractivity differences only occasionally exceeding  $\pm 10$  N-units. At the top of the time series plot, black circles indicate stable conditions with  $Ri > 0.25$  and red circles indicate unstable conditions with  $Ri < -1$ . The green horizontal line is plotted to show  $Ri=0.25$ . . . . . 47
- 10 Monthly histograms of the diurnal ranges of refractivity difference for KTLX in 2009. The diurnal range of refractivity differences is greatest in the warm season, with a median diurnal range exceeding 10 N-units in June and July 2009. The diurnal range of refractivity differences are much lower in the cool season, with median ranges between 3 – 6 N-units. The number of days with very large diurnal ranges of refractivity differences ( $>20$  N-units) is also much higher in the warm season than the cool season. . . . . 48

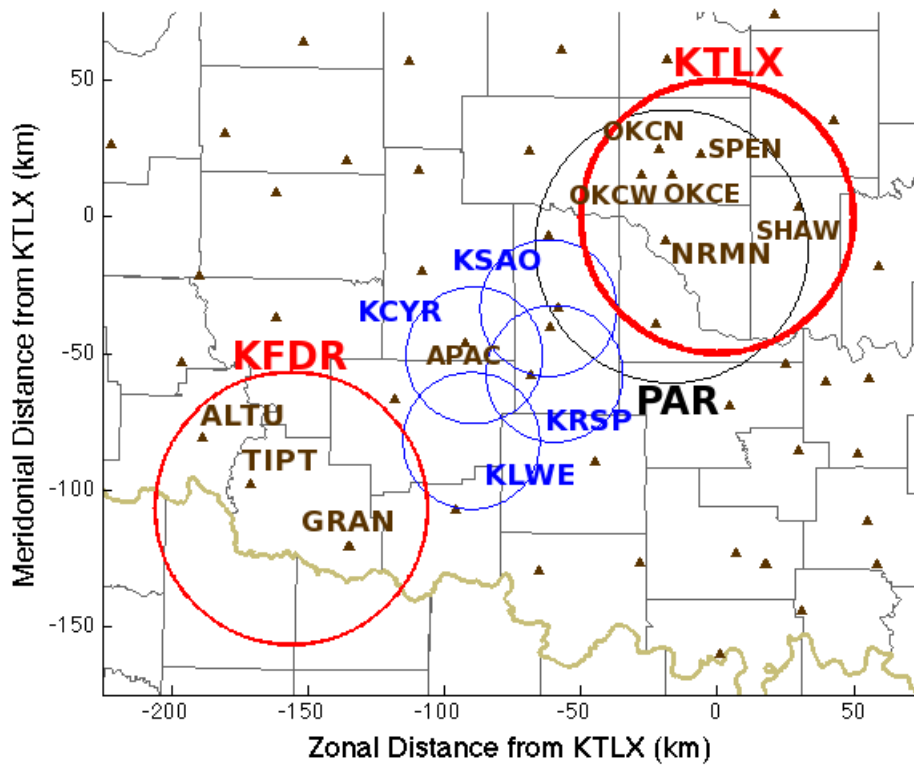


Figure 1: A map of radars used for refractivity retrieval in central and southwestern Oklahoma. Refractivity domains are colored based on radar type: WSR-88D (red), CASA (blue), and PAR (black). Oklahoma Mesonet stations are labeled in brown and shown by the brown triangles.

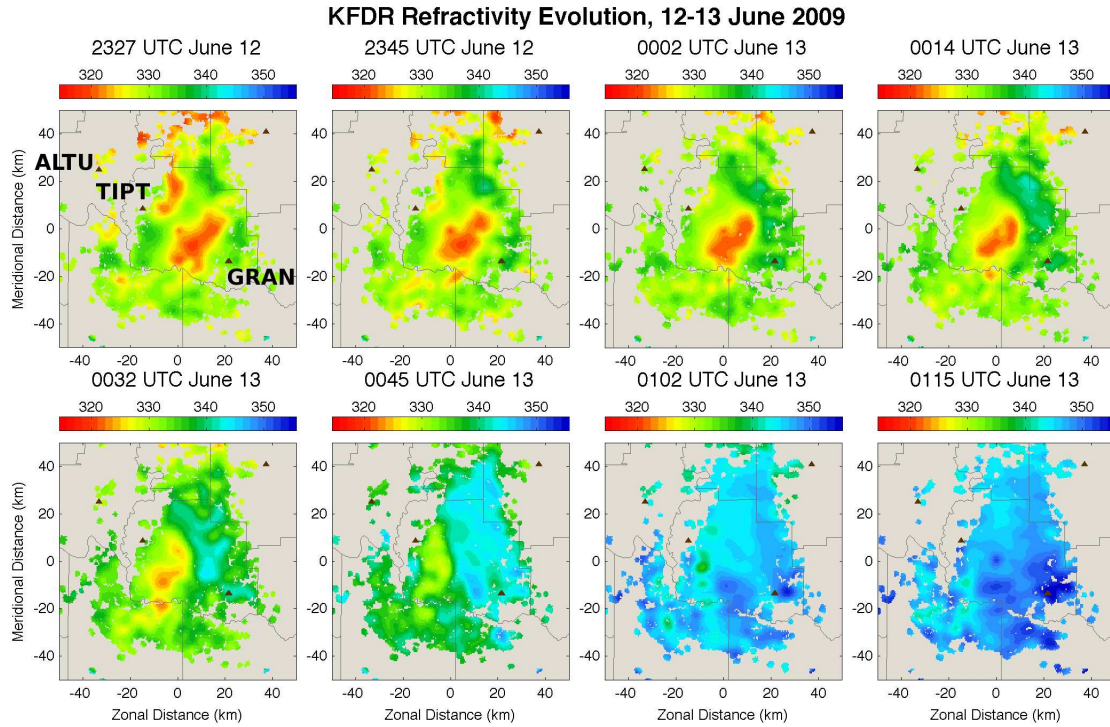


Figure 2: A two-hour evolution of radar refractivity fields, using KFDR in southwest Oklahoma. Radar scans were taken every 4–5 min during this time period; for brevity, scans at 15-min intervals are shown. Notice the rapid return of much higher refractivity from the east after 0000 UTC (1900 LT). The locations of the Altus (ALTU), Tipton (TIPT), and Grandfield (GRAN) Mesonet stations are demarcated by the black triangles.

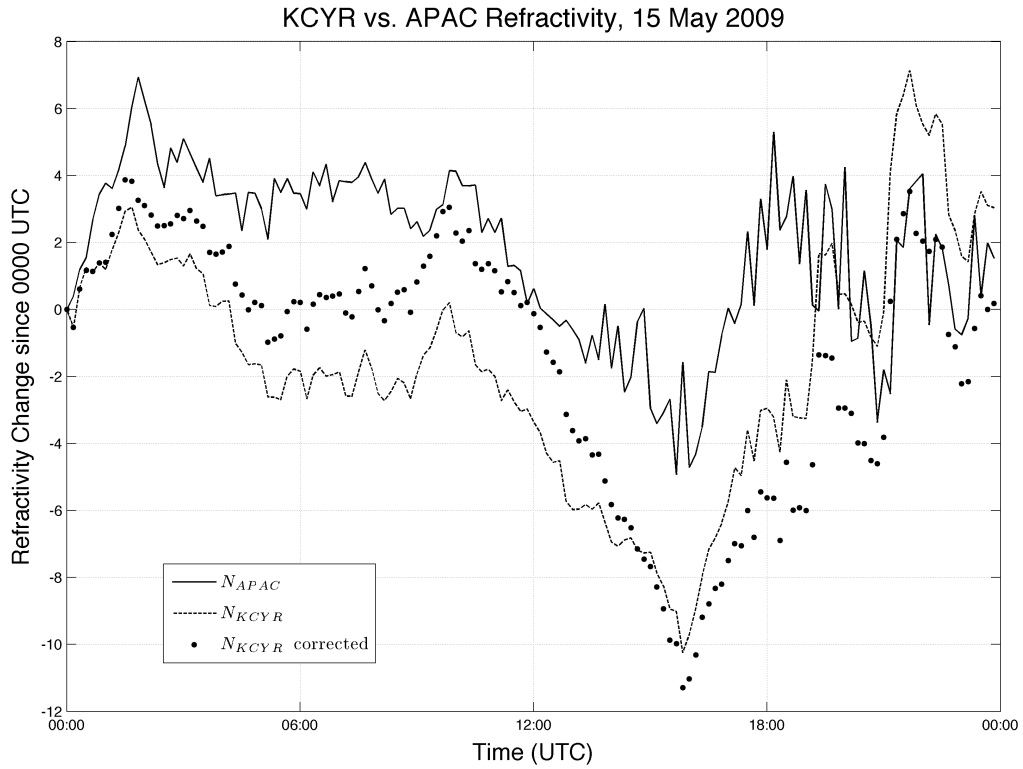


Figure 3: A comparison of sampled refractivity change, as derived from KCYR and the 2-m measurements from APAC, including frequency drift-corrected KCYR refractivity change. Refractivity difference is small during this period, with much of the difference being removed when correcting the data for the drift of the radar transmitter frequency.

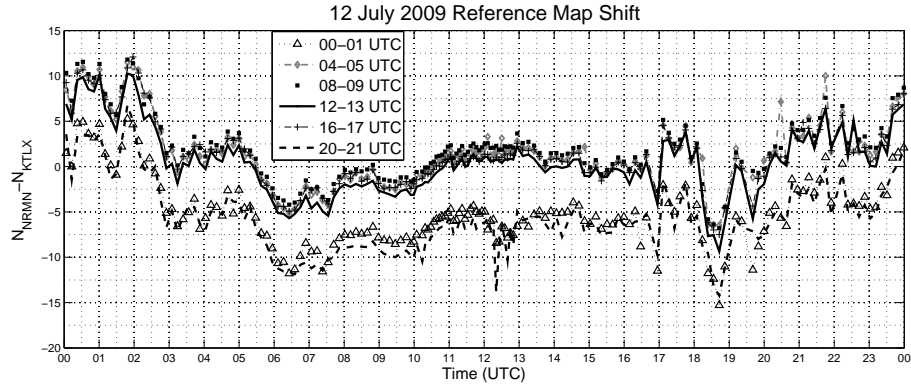


Figure 4: A time series comparison of the radar refractivity difference between the 2-m Norman Mesonet and radar refractivity, computed for six different reference maps. The reference maps were created at six different times on 12 July 2009, and the time series shown is on 12 July 2009. The reference maps are clustered into two separate groups based on the time of day. The reference maps made overnight and during the morning (0400 – 1600 UTC), and reference maps made in the afternoon and early evening (2000 – 0000 UTC) are clustered. The reference map can “shift” refractivity estimates as much as 7 N-units depending on the choice of reference map.

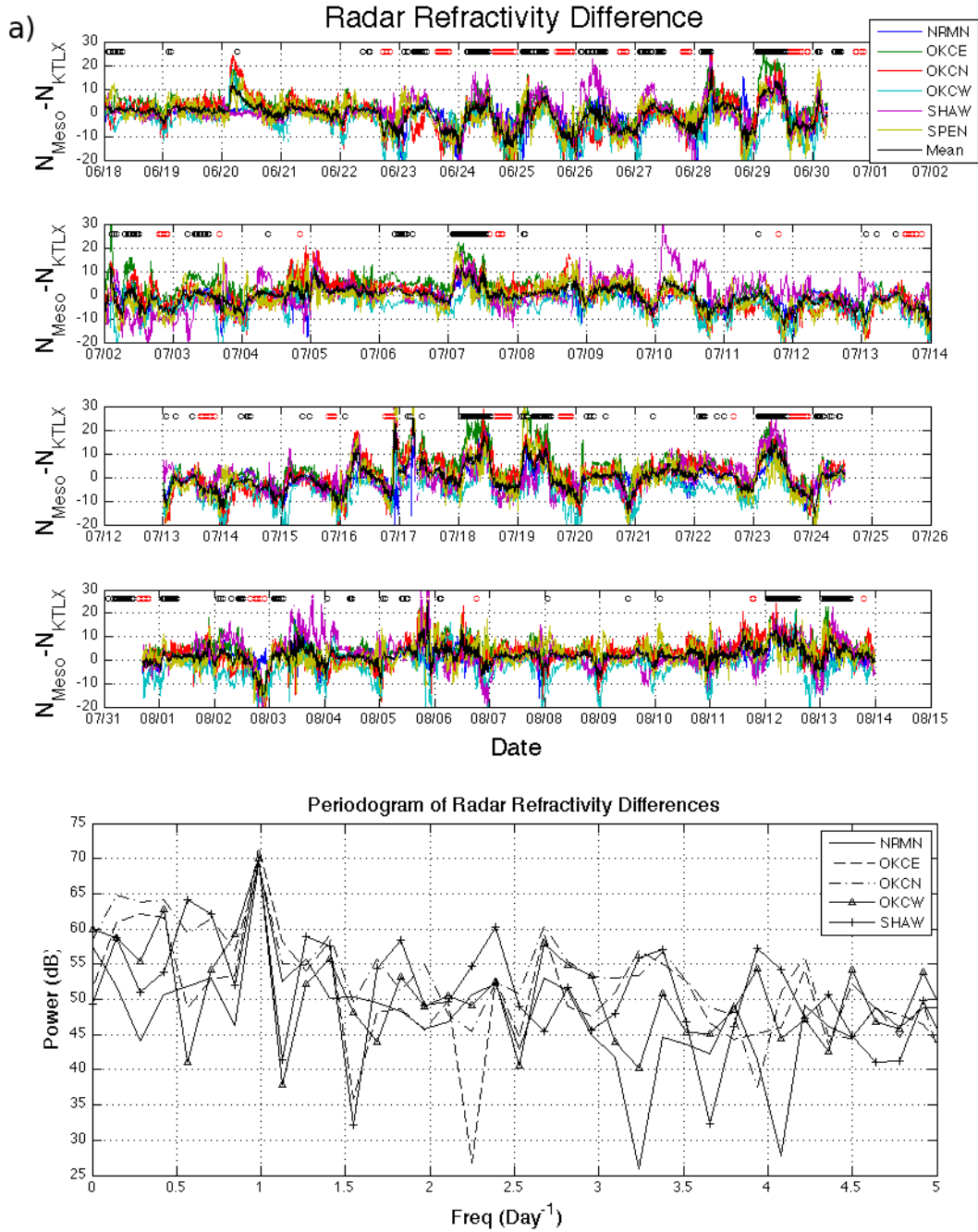


Figure 5: a) Time series of radar refractivity difference for six Mesonet stations, showing the difference between the 2-m Mesonet and radar refractivity between 18 Jun – 13 Aug 2009, and b) periodogram of radar refractivity difference between 18 Jun – 13 Aug 2009. The time series reveals a prominent diurnal periodicity in radar refractivity difference. At the top of the time series plot, black circles indicate stable conditions with  $Ri > 0.25$  and red circles indicate unstable conditions with  $Ri < -1$ . When a large diurnal range of radar refractivity difference occurs, the surface layer is stable at night and very unstable during the afternoon. In the periodogram, a prominent peak is observed at a frequency of  $1 \text{ day}^{-1}$  for each Mesonet station.

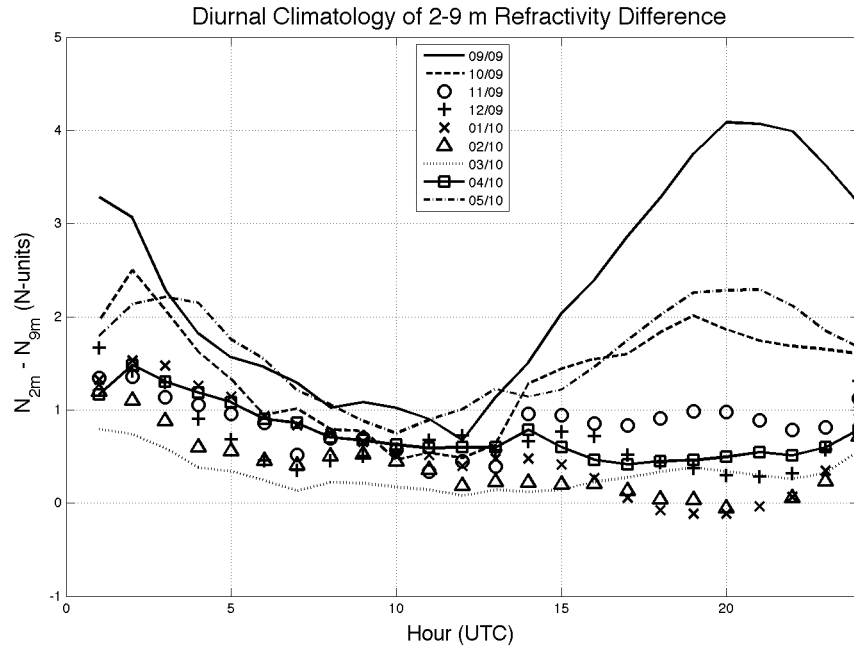


Figure 6: Climatology of the hourly mean refractivity difference between 2 and 9 m from the NRMN Mesonet site (difference in N-units). The plots show the monthly hourly mean from Sep 2009 to May 2010. Larger refractivity differences are observed in the warm season (e.g., 09/09 or 05/10), particularly in the late afternoon. In the cool season, the largest refractivity differences are observed overnight, owing to strong nocturnal inversions and increased dependence of refractivity on temperature (e.g., 01/10).

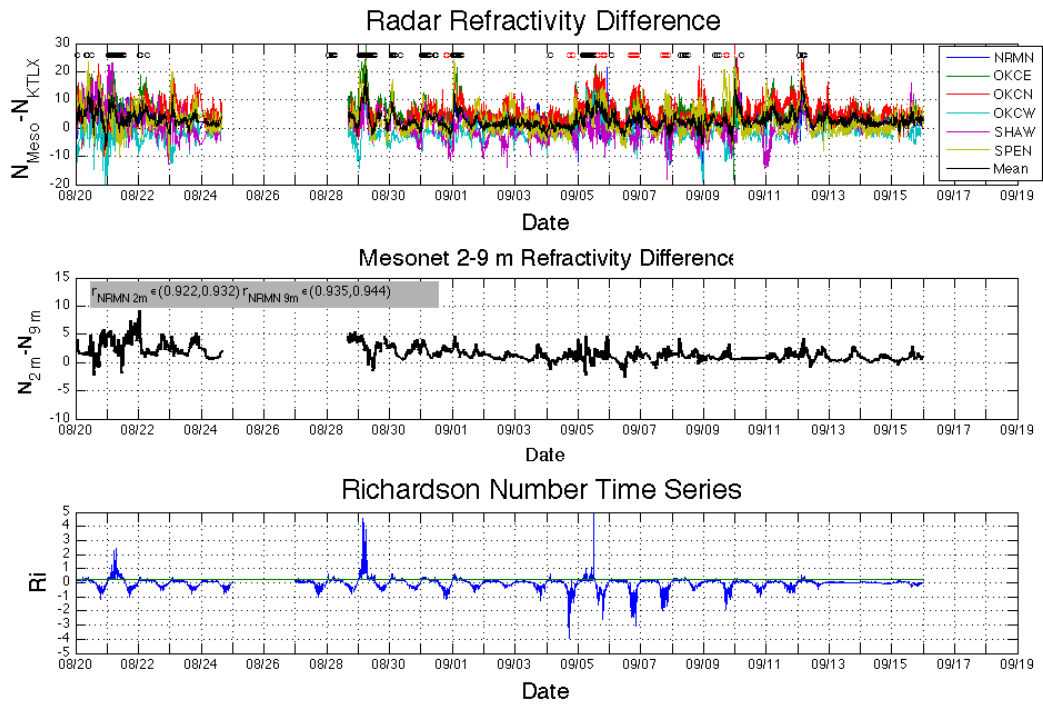


Figure 7: Time series of radar refractivity difference for six Mesonet stations, showing the difference between the 2-m Mesonet and radar refractivity between 20 Aug – 15 Sep 2009. At the top of the time series plot, black circles indicate stable conditions with  $Ri > 0.25$  and red circles indicate unstable conditions with  $Ri < -1$ . The green horizontal line is plotted to show  $Ri=0.25$ .

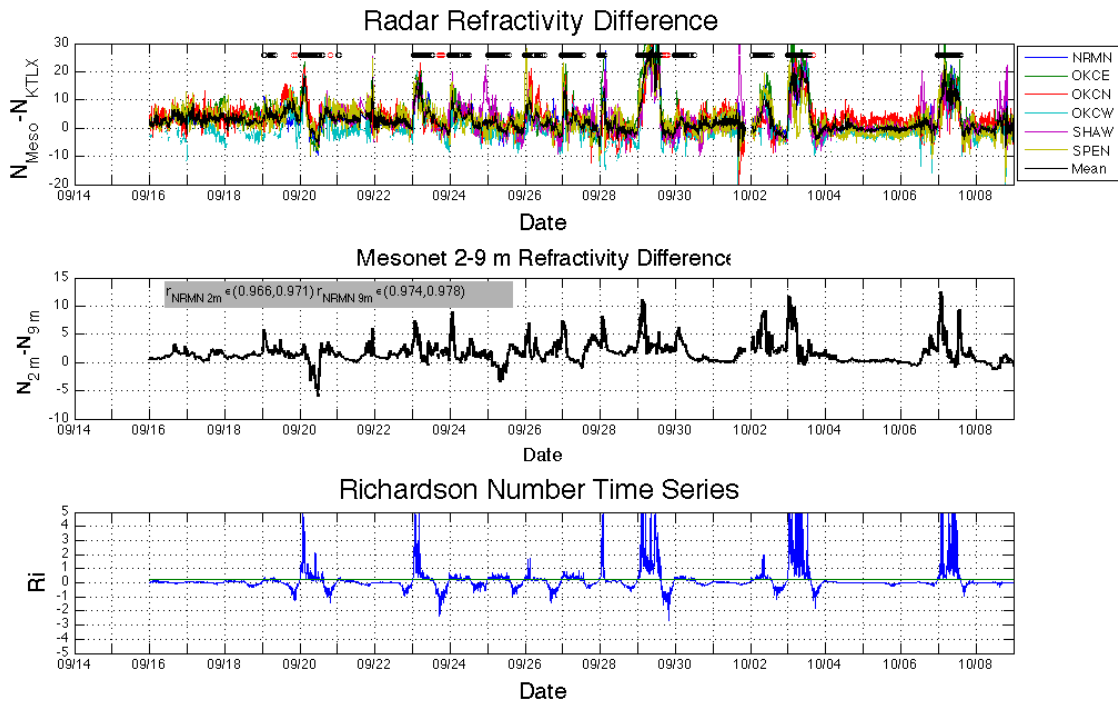


Figure 8: Time series of radar refractivity difference for six Mesonet stations, showing the difference between the 2-m Mesonet and radar refractivity between 16 Sep – 09 Oct 2009. At the top of the time series plot, black circles indicate stable conditions with  $Ri > 0.25$  and red circles indicate unstable conditions with  $Ri < -1$ . The green horizontal line is plotted to show  $Ri=0.25$ .

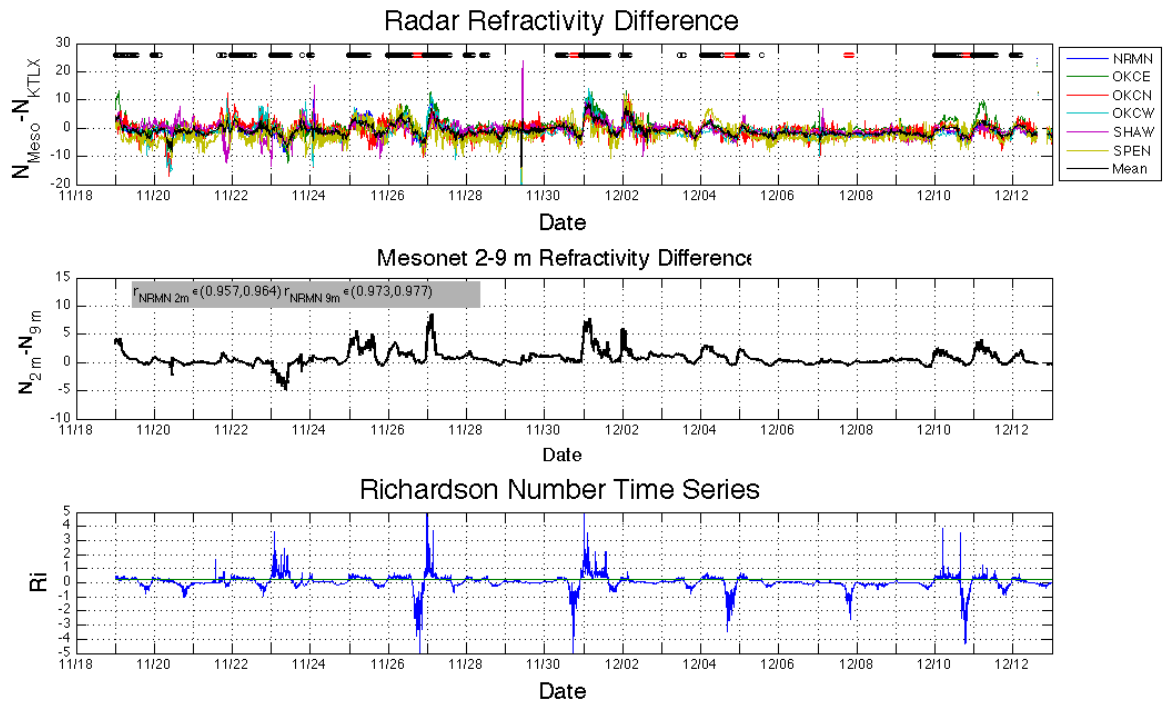


Figure 9: Time series of radar refractivity difference for six Mesonet stations, showing the difference between the 2-m Mesonet and radar refractivity between 19 Nov – 13 Dec 2009. In general, radar refractivity differences are much smaller in the cool season compared to the warm season, with radar refractivity differences only occasionally exceeding  $\pm 10$  N-units. At the top of the time series plot, black circles indicate stable conditions with  $Ri > 0.25$  and red circles indicate unstable conditions with  $Ri < -1$ . The green horizontal line is plotted to show  $Ri=0.25$ .

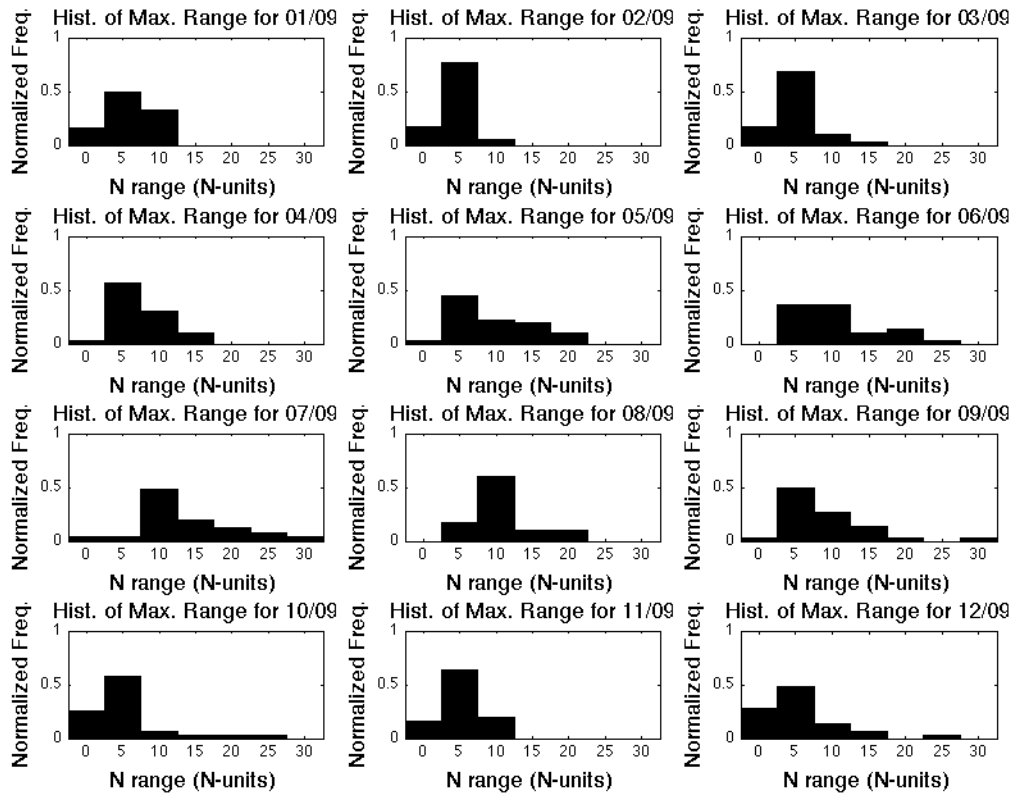


Figure 10: Monthly histograms of the diurnal ranges of refractivity difference for KTLX in 2009. The diurnal range of refractivity differences is greatest in the warm season, with a median diurnal range exceeding 10 N-units in June and July 2009. The diurnal range of refractivity differences are much lower in the cool season, with median ranges between 3 – 6 N-units. The number of days with very large diurnal ranges of refractivity differences ( $>20$  N-units) is also much higher in the warm season than the cool season.

# List of Tables

1	Radar refractivity error sources discussed in previous studies. The examples by Fabry (2004) are at 25 km range. . . . .	50
2	Examples of the impact of changes in vertical refractivity gradients on refractivity values and refractivity differences, $\epsilon$ , for heights, $h$ , of 10 and 20 m. The 2-m surface observation is always 300 N-units, and the vertical refractivity gradient at the reference time, $\frac{dN}{dz}$ at $t_{ref}$ , is -0.1 and -0.5 N-units $m^{-1}$ for the small and large gradient cases, respectively. $N(h=10\text{ m})$ and $N(h=20\text{ m})$ are the actual refractivity values at the measurement height, and $N_{radar}(h=10\text{ m})$ and $N_{radar}(h=20\text{ m})$ are the refractivity values obtained using the reference map. At the reference time, $t_{ref}$ , the 2-m surface observations and the radar are set equal. . . . .	51
3	Median monthly diurnal range, $\overline{R}$ , of radar refractivity difference (N-units) for KTLX between Mar 2008 – Apr 2010. . . . .	52
4	Median monthly KOUN radiosonde surface layer refractivity gradient (N-units $m^{-1} \times 10^{-1}$ ) between Mar 2008 – Apr 2010. A median radiosonde value for Dec 2008 was not computed because insufficient days with surface layer measurements were available (DM). . . . .	53

Table 1: Radar refractivity error sources discussed in previous studies. The examples by Fabry (2004) are at 25 km range.

<b>Error Source</b>	<b>Study</b>	<b>Magnitude (N-units)</b>
Vegetation sway	Fabry (2004)	$\pm 10$
Change in target shape from anomalous propagation	Fabry (2004)	$\pm 1$
Path change due to anomalous propagation	Fabry (2004)	$\pm 0.4$
Precipitation delay (10 – 100 mm hr <sup>-1</sup> )	Bodine et al. (2009)	1 – 7
Transmitter frequency drift (klystron)	Roberts et al. (2008)	0.4

Table 2: Examples of the impact of changes in vertical refractivity gradients on refractivity values and refractivity differences,  $\epsilon$ , for heights,  $h$ , of 10 and 20 m. The 2-m surface observation is always 300 N-units, and the vertical refractivity gradient at the reference time,  $\frac{dN}{dz}$  at  $t_{ref}$ , is -0.1 and -0.5 N-units  $m^{-1}$  for the small and large gradient cases, respectively.  $N(h=10\text{ m})$  and  $N(h=20\text{ m})$  are the actual refractivity values at the measurement height, and  $N_{radar}(h=10\text{ m})$  and  $N_{radar}(h=20\text{ m})$  are the refractivity values obtained using each reference map. At the reference time,  $t_{ref}$ , the 2-m surface observations and the radar are set equal.

Case	Small $\frac{dN}{dz} \Big _{t=t_{ref}}$			Large $\frac{dN}{dz} \Big _{t=t_{ref}}$		
	$t_{ref}$	$t_1$	$t_2$	$t_{ref}$	$t_1$	$t_2$
$\frac{dN}{dz}$ (N-units $m^{-1}$ )	-0.1	-0.5	-1.0	-0.5	-0.1	-1.0
$N(h=2\text{ m})$	300	300	300	300	300	300
$N(h=10\text{ m})$	299.2	296	291	296	299.2	292
$N(h=20\text{ m})$	298.2	292	282	291	298.2	282
$N_{radar}(h=10\text{ m})$	300	296.8	292.8	300	303.2	296
$N_{radar}(h=20\text{ m})$	300	292.8	<b>283.8</b>	300	307.2	<b>291</b>
$\epsilon(h=10\text{ m})$	0	3.2	7.2	0	-3.2	4
$\epsilon(h=20\text{ m})$	0	7.2	16.2	0	<b>-7.2</b>	<b>9</b>

Table 3: Median monthly diurnal range,  $\overline{R}$ , of radar refractivity difference (N-units) for KTLX between Mar 2008 – Apr 2010.

Year	Jan	Feb	Mar	Apr	May	Jun	Jul	Aug	Sep	Oct	Nov	Dec
2008	-	-	4.0	6.5	7.6	5.3	9.4	9.4	7.1	6.4	7.2	6.2
2009	5.6	3.5	4.2	6.2	9.2	10.1	11.8	8.7	7.3	3.7	5.2	3.8
2010	4.2	4.7	5.4	6.3	-	-	-	-	-	-	-	-

Table 4: Median monthly KOUN radiosonde surface layer refractivity gradient (N-units  $\text{m}^{-1} \times 10^{-1}$ ) between Mar 2008 – Apr 2010. A median radiosonde value for Dec 2008 was not computed because insufficient days with surface layer measurements were available (DM).

Year	Jan	Feb	Mar	Apr	May	Jun	Jul	Aug	Sep	Oct	Nov	Dec
2008	-	-	-0.48	-0.66	-1.04	-1.38	-1.30	-1.19	-0.98	-0.60	-0.32	DM
2009	-0.34	-0.42	-0.58	-0.63	-0.94	-0.91	-1.37	-1.13	-1.01	-0.76	-0.45	-0.33
2010	-0.39	-0.52	-0.46	-0.85	-	-	-	-	-	-	-	-